

A Fast Semi-Implicit Finite-Difference Method for the TDGL Equations

T. Winiecki and C. S. Adams

*Department of Physics, University of Durham, Rochester Building, South Road, Durham,
DH1 3LE, United Kingdom*

Received June 14, 2001; revised March 5, 2002

We propose a finite-difference algorithm for solving the time-dependent Ginzburg–Landau (TDGL) equation coupled to the appropriate Maxwell equation. The time derivatives are discretized using a second-order semi-implicit scheme which, for intermediate values of the Ginzburg–Landau parameter κ , allows time steps two orders of magnitude larger than commonly used in explicit schemes. We demonstrate the use of the method by solving a fully three-dimensional problem of a current-carrying wire with longitudinal and transverse magnetic fields. © 2002 Elsevier Science (USA)

Key Words: TDGL; superconductor.

1. GINZBURG–LANDAU MODEL

In the Ginzburg–Landau model, a superconductor is characterised by a complex order parameter ψ . The local density of superconducting electrons is represented by $|\psi|^2$. The theory postulates that close to the critical temperature, the free energy can be expanded in a series of the form

$$\begin{aligned} \mathcal{L}(\psi, \nabla\psi, \mathbf{A}, \nabla \times \mathbf{A}) = & a|\psi|^2 + \frac{1}{2}b|\psi|^4 + \frac{\hbar^2}{2m_s} \left| \left(\nabla - i\frac{e_s}{\hbar}\mathbf{A} \right) \psi \right|^2 \\ & + \frac{1}{2\mu_0} |\nabla \times \mathbf{A} - \mu_0\mathbf{H}|^2, \end{aligned} \quad (1)$$

where a and b are phenomenological parameters that depend on external parameters such as temperature, \mathbf{A} denotes the vector potential, \mathbf{H} is an external magnetic field, and e_s and m_s are the effective charge and the effective mass of the Cooper pairs. Below the transition temperature T_c , a becomes negative, whereas $b > 0$ for all T .

1.1. The Time-Dependent Ginzburg–Landau (TDGL) Equations

The equations of motion for the order parameter and the vector potential are the Euler–Lagrange equations of the free energy functional,

$$\frac{\hbar^2}{2m_s D} \left(\partial_t + i \frac{e_s}{\hbar} \Phi \right) \psi = \frac{\hbar^2}{2m_s} \left(\nabla - i \frac{e_s}{\hbar} \mathbf{A} \right)^2 \psi + |a|\psi - b|\psi|^2 \psi, \quad (2)$$

$$\frac{1}{\mu_0} \nabla \times (\nabla \times \mathbf{A} - \mu_0 \mathbf{H}) = \mathbf{j}_s + \mathbf{j}_n, \quad (3)$$

$$\mathbf{j}_s = \frac{\hbar e_s}{2m_s i} (\psi^* \nabla \psi - \psi \nabla \psi^*) - \frac{e_s^2}{m_s} |\psi|^2 \mathbf{A}, \quad (4)$$

$$\mathbf{j}_n = \sigma (-\nabla \Phi - \partial_t \mathbf{A}), \quad (5)$$

where D is a phenomenological diffusion constant and Φ is the electric potential, included to retain the gauge invariance of the equations. Equation (3) is the Maxwell equation for the magnetic field, where the displacement current $\epsilon_0 \dot{\mathbf{E}}$ has been omitted, as it only becomes significant for velocities close to the speed of light. The total current is given by the sum of the supercurrent, \mathbf{j}_s , and the normal current, \mathbf{j}_n , which obeys Ohm's law.

1.2. Dimensionless Units

We scale length in multiples of the coherence length, $\xi = \hbar / \sqrt{2m|a|}$, time in $\tau = \xi^2 / D$, the wavefunction in $\psi_0 = \sqrt{|a|/b}$, the vector potential in $A_0 = \sqrt{2\kappa H_c \xi}$, where $H_c = \mu_0 |a|^2 / b$, the electric potential in $\Phi_0 = (\xi / \tau) A_0$, and resistivity in units of the normal resistivity $\sigma_0 = 1 / \kappa^2 D \mu_0$. The so-called Ginzburg–Landau parameter is given by $\kappa^2 = 2m^2 b / e^2 \hbar^2 \mu_0$. The characteristic length scale for variations of the magnetic field is $\lambda = \kappa \xi$, and $\nabla \times \mathbf{A}$ measures the magnetic field in units of $\sqrt{2\kappa} H_c = H_{c2}$. In scaled units Eqs. (2) and (3) become

$$(\partial_t + i\Phi) \psi = (\nabla - i\mathbf{A})^2 \psi + \psi - |\psi|^2 \psi, \quad (6)$$

$$\kappa^2 \nabla \times \nabla \times \mathbf{A} = \underbrace{(\nabla S - \mathbf{A}) |\psi|^2}_{\mathbf{j}_s} + \underbrace{\sigma (-\nabla \Phi - \partial_t \mathbf{A})}_{\mathbf{j}_n} + \underbrace{\kappa^2 \nabla \times \mathbf{H}}_{\mathbf{j}_{ext}}, \quad (7)$$

where S denotes the phase of ψ . The last term in Eq. (7) can be understood as an external current \mathbf{j}_{ext} with $\nabla \mathbf{j}_{ext} = 0$. In the following, this term is omitted. However, it can be easily included in the algorithm for instance to model magnetic impurities. In dimensionless units, the dynamics of the superconductor depends on the dimensionless Ginzburg–Landau parameter κ only. For values $\kappa < 1/\sqrt{2}$ one finds a behaviour characteristic of a type-I superconductor whereas for $\kappa > 1/\sqrt{2}$ a type-II superconductor is modelled.

1.3. Gauge Transformation

The dynamics of the measurable quantities \mathbf{E} , \mathbf{B} , $|\psi|^2$, and \mathbf{j} are invariant under the transformation

$$\begin{cases} \mathbf{A} \rightarrow \mathbf{A} + \nabla \Lambda \\ \psi \rightarrow \psi e^{i\Lambda} \\ \Phi \rightarrow \Phi - \dot{\Lambda}, \end{cases} \quad (8)$$

where Λ is an arbitrary scalar field. We choose the zero potential gauge, $\Lambda(\mathbf{r}, t) = \int dt \Phi$

(\mathbf{r}, t) ; in other words, $\Phi(\mathbf{r}) \equiv 0$ at all times. For this choice, Eqs. (6) and (7) become

$$\partial_t \psi = (\nabla - i\mathbf{A})^2 \psi + \psi - |\psi|^2 \psi, \quad (9)$$

$$\sigma \partial_t \mathbf{A} = (\nabla S - \mathbf{A})|\psi|^2 - \kappa^2 \nabla \times \nabla \times \mathbf{A}. \quad (10)$$

In the following section, we suggest a fast and reliable numerical method to find an approximate solution to these equations.

2. NUMERICAL METHODS

The most popular approach to the solution of the TDGL equations, (9) and (10), is a gauge-invariant discretization that is second-order accurate in space and first order in time [1–5]. In addition, a number of other finite-difference [6, 7] and finite-element methods [8, 9] have been developed. For large values of κ , the magnetic field is nearly homogeneous and Eq. (10) can be dropped. This case is often referred to as the London limit. The remaining equation has been solved by a semi-implicit Fourier spectral method which is second-order accurate in time [10]. An equation very similar to Eq. (9), the Gross–Pitaevskii equation, is used to model vortex dynamics in dilute Bose–Einstein condensates [11]. Here, we modify the very robust and accurate semi-implicit Crank–Nicholson algorithm used in [11] to include the equation for the vector potential.

2.1. The U - ψ Method

The widely used U - ψ method is described in detail by Gropp *et al.* [1]. As this method forms the basis of our algorithm we briefly review the main points here. Complex link variables U^x , U^y , and U^z are introduced to preserve the gauge-invariant properties of the discretized equations.

$$\begin{aligned} U^x(x, y, z) &= \exp\left(-i \int_{x_0}^x A^x(x', y, z) dx'\right), \\ U^y(x, y, z) &= \exp\left(-i \int_{y_0}^y A^y(x, y', z) dy'\right), \\ U^z(x, y, z) &= \exp\left(-i \int_{z_0}^z A^z(x, y, z') dz'\right), \end{aligned} \quad (11)$$

where (x_0, y_0, z_0) is an arbitrary reference point. The TDGL equations can then be expressed as functions of ψ and these link variables. Both the order parameter and the link variables are discretized on a three-dimensional grid with grid spacing h_x , h_y , and h_z , respectively. The mesh points for the link variables are half way between the mesh points for the order parameter (see Fig. 1). All spatial derivatives are approximated by finite differences to second-order accuracy. Denoting the complex conjugate of U by \bar{U} , the finite-difference representations of the TDGL equations read

$$\begin{aligned} \partial_t \psi_{i,j,k} &= \frac{\bar{U}_{i-1,j,k}^x \psi_{i-1,j,k} - 2\psi_{i,j,k} + U_{i,j,k}^x \psi_{i+1,j,k}}{h_x^2} \\ &+ \frac{\bar{U}_{i,j-1,k}^y \psi_{i,j-1,k} - 2\psi_{i,j,k} + U_{i,j,k}^y \psi_{i,j+1,k}}{h_y^2} \\ &+ \frac{\bar{U}_{i,j,k-1}^z \psi_{i,j,k-1} - 2\psi_{i,j,k} + U_{i,j,k}^z \psi_{i,j,k+1}}{h_z^2} + (1 - |\psi_{i,j,k}|^2) \psi_{i,j,k}, \end{aligned} \quad (12)$$

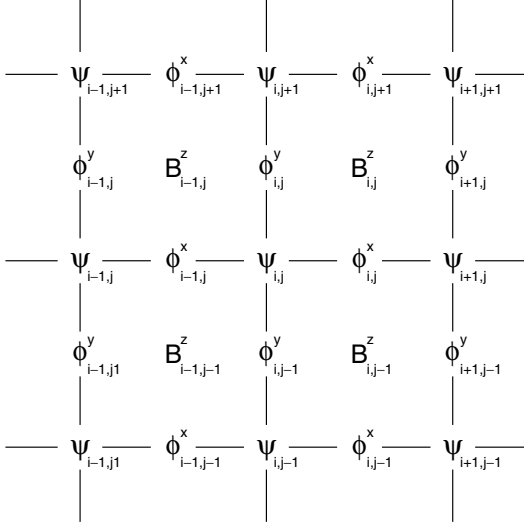


FIG. 1. The evaluation points for the fields ψ and ϕ in the x - y plane. A finite-difference approximation for the magnetic field B_z is given in (36).

$$\partial_t U_{i,j,k}^x = -i \operatorname{Im}(\mathcal{F}_{i,j,k}^x) U_{i,j,k}^x, \quad (13)$$

where

$$\begin{aligned} \mathcal{F}_{i,j,k}^x &= \kappa^2 \frac{\bar{U}_{i,j+1,k}^x \bar{U}_{i,j,k}^y U_{i,j,k}^x U_{i+1,j,k}^y - \bar{U}_{i,j,k}^x \bar{U}_{i,j-1,k}^y U_{i,j-1,k}^x U_{i+1,j-1,k}^y}{h_y^2} \\ &+ \kappa^2 \frac{\bar{U}_{i+1,j,k-1}^z \bar{U}_{i,j,k-1}^x U_{i,j,k-1}^z U_{i,j,k}^x - \bar{U}_{i+1,j,k}^z \bar{U}_{i,j,k}^x U_{i,j,k}^z U_{i,j,k+1}^x}{h_z^2} \\ &+ U_{i,j,k}^x \bar{\Psi}_{i,j,k} \Psi_{i+1,j,k}. \end{aligned}$$

Analogous expressions for $\partial_t U_{i,j,k}^y$ and $\partial_t U_{i,j,k}^z$ can be obtained by permutating the coordinates and indices as follows:

$$(x, y, z; i, j, k) \rightarrow (y, z, x; j, k, i) \rightarrow (z, x, y; k, i, j) \rightarrow (x, y, z; i, j, k). \quad (14)$$

The time evolution is approximated by a simple Euler step,

$$\psi_{i,j,k}(t + \Delta t) = \psi_{i,j,k}(t) + \Delta t \partial_t \psi_{i,j,k}(t) + \mathcal{O}(\Delta t^2), \quad (15)$$

$$U_{i,j,k}^x(t + \Delta t) = U_{i,j,k}^x(t) + \Delta t \partial_t U_{i,j,k}^x(t) + \mathcal{O}(\Delta t^2). \quad (16)$$

To keep $U_{i,j,k}^x$ unimodular, Eq. (16) is often modified to

$$U_{i,j,k}^x(t + \Delta t) = U_{i,j,k}^x(t) \exp(-i \Delta t \operatorname{Im} \mathcal{F}_{i,j,k}^x) + \mathcal{O}(\Delta t^2). \quad (17)$$

The Euler method is only first-order accurate in time, i.e., the truncation error made due to the finite-difference approximation of the time derivative is proportional to Δt^2 . However, the main problem is that the code becomes unstable if long time steps are used. The cause of

this instability is the diffusionlike character of the dynamics described by Eqs. (12) and (13). Equation (12) can immediately be written as a diffusion equation with an additional nonlinear term,

$$\partial_t \psi_{i,j,k} = L_x \psi_{i,j,k} + L_y \psi_{i,j,k} + L_z \psi_{i,j,k} + f, \quad (18)$$

where f stands for $(1 - |\psi_{i,j,k}|^2)\psi_{i,j,k}$ and L_x , L_y , and L_z denote the *weighted* Laplacian operators,

$$L_x \psi_{i,j,k} \equiv \frac{a_{i-1} \psi_{i-1,j,k} - 2\psi_{i,j,k} + a_{i+1} \psi_{i+1,j,k}}{h_x^2}, \quad (19)$$

with $|a_{i-1}| = |a_{i+1}| = 1$ in our case. The diffusion constant is 1 in dimensionless units. Equation (13) is also dominated by diffusive terms, as becomes evident in the next section. Setting $\sigma = 1$, the diffusion constant for the vector potential is κ^2 . This can be seen by taking the curl of Eq. (10), $\dot{\mathbf{B}} = \kappa^2 \nabla^2 \mathbf{B} + \nabla \times \mathbf{j}_s$. The one-step forward Euler method is only stable as long as the time step is shorter than the diffusion time across a cell of width h [13]. For example, using a grid spacing of $h = 0.5\xi$ and $\kappa = 4$, the theoretical limit for the time step is

$$\Delta t < \frac{h^2}{2\kappa^2} = \frac{0.5^2}{2 \cdot 4^2} \approx 0.0078. \quad (20)$$

In practice, a time step of $\Delta t = 0.0025$ is used to ensure stability [1]. In contrast, a semi-implicit two-step algorithm is unconditionally stable for diffusive problems and enables much larger time steps to be employed.

2.2. Semi-implicit Algorithm

We propose a spatial discretization of the equations very similar to the above U - ψ method. The link variables are unimodular, $|U_{i,j,k}^x| = 1$, and can be written as the exponential of a phase, $U_{i,j,k}^x = \exp(-i\phi_{i,j,k}^x)$. We use the real-valued variable ϕ^x instead of the complex-valued U^x . The fields ψ and ϕ are represented on a three-dimensional grid. The mesh points of the phase factors are placed between the mesh points of the order parameter (see Fig. 1). For the field $\psi_{i,j,k}$, the grid point indices are $i = 1 \dots N_x + 1$, $j = 1 \dots N_y + 1$, and $k = 1 \dots N_z + 1$. For $\phi_{i,j,k}^x$, the indices in the x direction are in the range $i = 1 \dots N_x$ only, due to the relative displacement of the grids. Similarly, $j = 1 \dots N_y$ for $\phi_{i,j,k}^y$ and $k = 1 \dots N_z$ for $\phi_{i,j,k}^z$.

We now discretize the spatial derivatives in Eqs. (9) and (10) using the modified link variables ϕ^x , ϕ^y , and ϕ^z . For Eq. (9), we reuse the expansion (12) except that we replace $U_{i,j,k}^x$ with $\exp(-i\phi_{i,j,k}^x)$, and so forth:

$$\begin{aligned} \partial_t \psi_{i,j,k} = & \frac{\exp(i\phi_{i-1,j,k}^x) \psi_{i-1,j,k} - 2\psi_{i,j,k} + \exp(-i\phi_{i,j,k}^x) \psi_{i+1,j,k}}{h_x^2} \\ & + \frac{\exp(i\phi_{i,j-1,k}^y) \psi_{i,j-1,k} - 2\psi_{i,j,k} + \exp(-i\phi_{i,j,k}^y) \psi_{i,j+1,k}}{h_y^2} \\ & + \frac{\exp(i\phi_{i,j,k-1}^z) \psi_{i,j,k-1} - 2\psi_{i,j,k} + \exp(-i\phi_{i,j,k}^z) \psi_{i,j,k+1}}{h_z^2} \\ & + (1 - |\psi_{i,j,k}|^2) \psi_{i,j,k}. \end{aligned} \quad (21)$$

With the help of the relation $-\nabla \times \nabla \times \mathbf{A} = \nabla^2 \mathbf{A} - \nabla(\nabla \mathbf{A})$, the second-order-accurate finite-difference representation of (10) is

$$\begin{aligned}
\partial_t \phi_{i,j,k}^x &= \frac{\kappa^2}{h_y^2} (\phi_{i,j+1,k}^x - 2\phi_{i,j,k}^x + \phi_{i,j-1,k}^x) + \frac{\kappa^2}{h_z^2} (\phi_{i,j,k+1}^x - 2\phi_{i,j,k}^x + \phi_{i,j,k-1}^x) \\
&+ \frac{\kappa^2}{h_y^2} (-\phi_{i+1,j,k}^y + \phi_{i,j,k}^y + \phi_{i+1,j-1,k}^y - \phi_{i,j-1,k}^y) \\
&+ \frac{\kappa^2}{h_z^2} (-\phi_{i+1,j,k}^z + \phi_{i,j,k}^z + \phi_{i+1,j,k-1}^z - \phi_{i,j,k-1}^z) \\
&+ \text{Im}(\exp(-i\phi_{i,j,k}^x) \bar{\Psi}_{i,j,k} \Psi_{i+1,j,k}). \tag{22}
\end{aligned}$$

The expressions for $\partial_t \phi_{i,j,k}^y$ and $\partial_t \phi_{i,j,k}^z$ are given by cyclic permutation (14).

Note that the discretized equations are still invariant under the gauge transformation:

$$\begin{cases} \psi_{i,j,k} \rightarrow \psi_{i,j,k} \exp(i\Lambda_{i,j,k}) \\ \phi_{i,j,k}^x \rightarrow \phi_{i,j,k}^x + (\Lambda_{i+1,j,k} - \Lambda_{i,j,k}) \\ \phi_{i,j,k}^y \rightarrow \phi_{i,j,k}^y + (\Lambda_{i,j+1,k} - \Lambda_{i,j,k}) \\ \phi_{i,j,k}^z \rightarrow \phi_{i,j,k}^z + (\Lambda_{i,j,k+1} - \Lambda_{i,j,k}). \end{cases} \tag{23}$$

Retaining the gauge invariance at the discrete level is often equivalent to preserving certain conservation laws and physical principles. It is crucial that the numerical approximation not depend on the particular choice of gauge. If, for example, one studies the motion of a vortex lattice due to an applied electric field E_x , the measurable quantities \mathbf{B} , $|\psi|^2$, and \mathbf{j} oscillate in time [16]. The system is driven through a series of equivalent solutions and the dynamics is roughly described by $\Lambda = E_x x t$. This means that the phase gradients in the order parameter build up in time and the phase difference between two neighbouring grid points eventually exceeds 2π . This is normally a problem as the finite-difference approximation becomes invalid. However, using the link variables U or ϕ these phase gradients are exactly cancelled by the change in the vector potential.

We now want to introduce a new scheme to update the wavefunction $\psi^{(n)}$ and the link variables $\phi^{(n)}$ from the n th to the $(n+1)$ th step. The idea is to treat the diffusive terms semi-implicitly whereas all other terms are still treated explicitly. In this way we reduce the stability constraints associated with the simple Euler method but avoid the expensive solution of nonlinear equations. The technique is known as *the method of fractional steps* [12]. A second-order accuracy in the time step can be achieved by a simple three-step iteration.

As mentioned above, the diffusive character of Eq. (10) becomes apparent in the new discretization and both Eq. (21) and Eq. (22) can be written as an initial value problem of the form

$$\partial_t u_{i,j,k} = D(L_x u_{i,j,k} + L_y u_{i,j,k} + L_z u_{i,j,k}) + f, \tag{24}$$

where u stands for the fields ψ or ϕ^x , ϕ^y or ϕ^z , respectively, D is the diffusion constant with $D = \kappa^2$ in (22), and f indicates all the other terms: $(1 - |\psi_{i,j,k}|^2)\psi_{i,j,k}$ in (21) and the last three lines in Eq. (22). Note that $L_x \equiv 0$ in (22).

The second derivatives are approximated in the usual way by an expression involving three neighbouring grid points. For any pair (j, k) the action of L_x on the vector $\{u_{i,j,k}\}_{i=2\dots N_x}$ can be represented by a tridiagonal matrix δ_x^2 ,

$$L_x u_{i,j,k} \equiv \frac{\delta_x^2}{h_x^2} u_{i,j,k} \equiv \frac{a_{i-1} u_{i-1,j,k} - 2u_{i,j,k} + a_{i+1} u_{i+1,j,k}}{h_x^2}. \quad (25)$$

As emphasized before, the instabilities of the Euler method have their origin in the explicit treatment of the diffusive terms. We now discretize the time derivative in Eq. (24) in the following way:

$$\begin{aligned} \frac{u^{(n+1)} - u^{(n)}}{\Delta t} &= \frac{1}{2} \frac{D\delta_x^2}{h_x^2} (u^{(n+1)} + u^{(n)}) + \frac{1}{2} \frac{D\delta_y^2}{h_y^2} (u^{(n+1)} + u^{(n)}) \\ &\quad + \frac{1}{2} \frac{D\delta_z^2}{h_z^2} (u^{(n+1)} + u^{(n)}) + \frac{1}{2} (f^{(n+1)} + f^{(n)}) + \mathcal{O}(\Delta t^2). \end{aligned} \quad (26)$$

This discretization is semi-implicit, as the right hand side of the equation depends on the fields at the old and the new time level. This mixing leads to an improved accuracy and prevents the algorithm from developing instabilities. After rearranging the equation we get

$$\begin{aligned} &\left(1 - \frac{D\Delta t}{2h_x^2} \delta_x^2 - \frac{D\Delta t}{2h_y^2} \delta_y^2 - \frac{D\Delta t}{2h_z^2} \delta_z^2\right) u^{(n+1)} \\ &= \left(1 + \frac{D\Delta t}{2h_x^2} \delta_x^2 + \frac{D\Delta t}{2h_y^2} \delta_y^2 + \frac{D\Delta t}{2h_z^2} \delta_z^2\right) u^{(n)} + \frac{\Delta t}{2} (f^{(n+1)} + f^{(n)}) + \mathcal{O}(\Delta t^3). \end{aligned} \quad (27)$$

We now employ an *approximate factorisation* [12],

$$\begin{aligned} &\left(1 - \frac{D\Delta t}{2h_x^2} \delta_x^2 - \frac{D\Delta t}{2h_y^2} \delta_y^2 - \frac{D\Delta t}{2h_z^2} \delta_z^2\right) \\ &= \left(1 - \frac{D\Delta t}{2h_x^2} \delta_x^2\right) \left(1 - \frac{D\Delta t}{2h_y^2} \delta_y^2\right) \left(1 - \frac{D\Delta t}{2h_z^2} \delta_z^2\right) + \mathcal{O}(\Delta t^2). \end{aligned} \quad (28)$$

The multidimensional operator is split into three operators that involve difference approximations in only one dimension. With the abbreviations

$$A_x = \left(1 - \frac{D\Delta t}{2h_x^2} \delta_x^2\right), \quad B_x = \left(1 + \frac{D\Delta t}{2h_x^2} \delta_x^2\right), \quad (29)$$

and considering $(u^{(n+1)} - u^{(n)}) = \mathcal{O}(\Delta t)$ Eq. (27) becomes

$$A_x A_y A_z u^{(n+1)} = B_x B_y B_z u^{(n)} + \frac{\Delta t}{2} (f^{(n+1)} + f^{(n)}) + \mathcal{O}(\Delta t^3). \quad (30)$$

The tridiagonal matrices A and B are actually time dependent because the differential operators L in Eq. (21) depend on the link variables. In the above equation, A is a function of $\phi^{(n+1)}$ whereas B depends on $\phi^{(n)}$. Consequently, the equations are solved in the stepwise

manner

$$\begin{aligned}
 A_x u^{(n+1/3)} &= B_x B_y B_z u^{(n)} + \frac{\Delta t}{2} (f^{(n+1)} + f^{(n)}), \\
 A_y u^{(n+2/3)} &= u^{(n+1/3)}, \\
 A_z u^{(n+1)} &= u^{(n+2/3)},
 \end{aligned}
 \tag{31}$$

where the ‘‘fractional’’ time levels indicate intermediate results. The explicit term $f^{(n+1)}$ as well as the matrix elements of A may depend on the values of the link variables at the new time level and are unknown initially. We assume that $u^{(n+1)} = u^{(n)}$ to start with. After the first iteration of Eq. (31) for *all* variables ψ and ϕ , the updated values at the new time level are used in the matrix elements of A for the second iteration, and so on. The product $B_x B_y B_z u^{(n)}$ is a function of known values at the previous time level and can be stored in an auxiliary variable for subsequent iterations. As the matrices A are tridiagonal, fast inversion routines can be applied [13].

The entire algorithm relies on the convergence of this iteration technique. To test whether the procedure converges, we calculate a total update, $S(m)$, of the fields after m iterations by comparing all values at the time level $(n + 1)$ to all values at the previous time step, (n) .

$$S(m) = \sum_{i,j,k} ((|\psi_{i,j,k}^{(n+1,m)}|^2 - |\psi_{i,j,k}^{(n)}|^2)^2 + (\phi_{i,j,k}^{x(n+1,m)} - \phi_{i,j,k}^{x(n)})^2 + \dots),
 \tag{32}$$

where the three dots indicate the corresponding terms for the fields ϕ^y and ϕ^z . Figure 2 shows a typical evolution of the update for a time step of $\Delta t = 0.5$. After as few as five iterations the approximated increment is very close to the exact value. For smaller time steps, the procedure converges faster. We find an optimum trade-off between accuracy and performance for three iterations. We further check to see if the correction between two

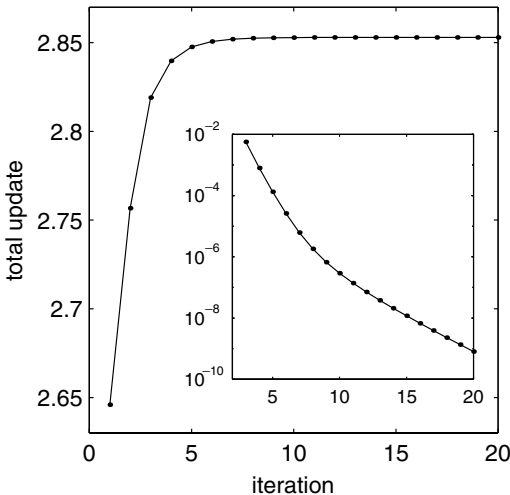


FIG. 2. The modification to the solution after one time step (total update) versus the number of iterations. For smaller time steps, the solution converges faster. We find an optimum of speed and accuracy for a combination of three iterations and a time step of $\Delta t = 0.5$. The correction between iterations, $T(m)$, is shown in the inset.

successive iterations,

$$T(m) = \sum_{i,j,k} ((|\Psi_{i,j,k}^{(n+1,m)}|^2 - |\Psi_{i,j,k}^{(n+1,m-1)}|^2)^2 + (\Phi_{i,j,k}^{x(n+1,m)} - \Phi_{i,j,k}^{x(n+1,m-1)})^2 + \dots), \quad (33)$$

converges to zero. Figure 2 (inset) confirms an exponential convergence.

The accuracy of the method is assessed by comparing the solution to simulations using the Euler method with a much smaller time step, $\Delta t = 0.0025$. Up to a time step of $\Delta t = 0.5$, no significant deviations could be observed. The program runs about 40 times faster than the Euler method for these parameters. For the calculations below we use a finer grid ($h = 0.4$) and a slightly larger Ginzburg–Landau parameter ($\kappa = 5$). The speedup for these values is about 100.

Our implicit method is less memory intensive than the standard U - ψ method because it uses real-valued link variables rather than complex-valued ones that must be represented by two real numbers. For a grid of N^3 points, the Euler method uses an equivalent of $22N^3$ real-valued variables (the complex wavefunction and the three complex link variables at two time levels plus three complex fields W ; see [1]) whereas the implicit method requires the storage of a total of $19N^3$ variables (the complex wavefunction and the three real link variables at two time levels, the products $B_x B_y B_z u^{(n)}$ in (31) plus four auxiliary fields).

2.3. Boundary Conditions

The correct implementation of the boundary conditions requires great care because of the relative displacement of the grids. The matrices A_x and B_x only act on the interior points, $i = 2 \dots N_x$, of the vectors ψ_i , ϕ_i^y , and ϕ_i^z for all $j = 1 \dots N_y + 1$, $k = 1 \dots N_z + 1$. Note that $A_x = B_x \equiv 1$ in the case $u = \phi^x$. The endpoints $i = 1$ and $i = N_x + 1$ are computed for bookkeeping purposes. Similarly, the operators B_y and B_z do not automatically include information on the endpoints at $j = 1$, $N_y + 1$ and $k = 1$, $N_z + 1$, respectively. In addition, there are different boundary conditions, namely periodic, Dirichlet, and Neumann, that require an adaption of the matrix elements on the first and last rows [13].

Another complication is that the physical boundary conditions that apply for the vectors $u^{(n)}$ and $u^{(n+1)}$ in Eq. (31) do not necessarily apply for the intermediate results $u^{(n+1/3)}$ and $u^{(n+2/3)}$. For example, when solving the second equation of the system (31),

$$A_y u^{(n+2/3)} = u^{(n+1/3)}, \quad (31')$$

a correct treatment of the boundary condition for $u^{(n+2/3)} = A_z u^{(n+1)}$ must be implemented into A_y . It is advisable to solve (31) starting in the direction with the simplest boundary condition. For a periodic boundary condition, for example, the relations $u_1 = u_N$ and $u_{N+1} = u_2$ hold at all time levels, including “fractional” ones.

The boundary conditions depend on the geometry of the problem. We choose a system with a periodic boundary condition in the z direction. At the interfaces in the x and the y directions, boundary conditions for the magnetic field and the order parameter are applied. For the order parameter $\psi_{i,j,k}$, conditions are needed for all values at the faces of the three-dimensional box. The grid representation of the periodic boundary condition reads

$$\begin{aligned} \psi_{i,j,1} &= \psi_{i,j,N_z}, & \psi_{i,j,N_z+1} &= \psi_{i,j,2}, \\ \phi_{i,j,1}^x &= \phi_{i,j,N_z}^x, & \phi_{i,j,N_z+1}^x &= \phi_{i,j,2}^x. \end{aligned} \quad (34)$$

In the y and z directions we set the supercurrent across the boundary to zero [1], i.e.,

$$\begin{aligned}
 \psi_{1,j,k} &= \psi_{2,j,k} \exp(-i\phi_{1,j,k}^x), \\
 \psi_{N_x+1,j,k} &= \psi_{N_x,j,k} \exp(+i\phi_{N_x,j,k}^x), \\
 \psi_{i,1,k} &= \psi_{i,2,k} \exp(-i\phi_{i,1,k}^y), \\
 \psi_{i,N_y+1,k} &= \psi_{i,N_y,k} \exp(+i\phi_{i,N_y,k}^y).
 \end{aligned} \tag{35}$$

Expressions for the endpoints of the link variables can be found by incorporating information about the magnetic field at the boundaries of the box. The three components of the magnetic field are given by the following second-order finite-difference approximations:

$$\begin{aligned}
 B_{i,j,k}^x &= \frac{1}{h_y h_z} (\phi_{i,j,k}^y - \phi_{i,j,k+1}^y - \phi_{i,j,k}^z + \phi_{i,j+1,k}^z), \\
 B_{i,j,k}^y &= \frac{1}{h_z h_x} (\phi_{i,j,k}^z - \phi_{i+1,j,k}^z - \phi_{i,j,k}^x + \phi_{i,j,k+1}^x), \\
 B_{i,j,k}^z &= \frac{1}{h_x h_y} (\phi_{i,j,k}^x - \phi_{i,j+1,k}^x - \phi_{i,j,k}^y + \phi_{i+1,j,k}^y).
 \end{aligned} \tag{36}$$

From these expressions, appropriate boundary conditions can be obtained. For example, the field $\phi_{i,j,k}^x$ is unknown at $j = 1$, and we use the last equation to relate the values of $\phi_{i,1,k}^x$ to known values

$$\phi_{i,1,k}^x = -B_{i,1,k}^z h_x h_y + \phi_{i,2,k}^x + \phi_{i,1,k}^y - \phi_{i+1,1,k}^y. \tag{37}$$

Equations (21), (22), and (31) combined with the boundary conditions (34), (35), and (37) provide all the information needed to solve a three-dimensional problem.

3. EXAMPLE 1: WIRE WITH LONGITUDINAL FIELD

As an example, we model an infinite cylindrical wire in three dimensions with an external magnetic field, H_z , applied along its axis. Such a configuration has been studied in [7, 14]. Experiments have shown that the magnetic field can increase the critical current down the wire [15].

In a type-II superconductor, a sufficiently strong magnetic field, H_z , will enter the cylinder and become trapped in vortex tubes aligned parallel to the axis of the cylinder. A current I along the wire induces an additional circular field $H_\varphi(\mathbf{r})$ such that $I = 2\pi\rho\kappa^2 H_\varphi(\rho)$ at a distance ρ from the axis of the wire. For $H_\varphi(\rho)$ we assume a perfect $1/r$ field corresponding to a constant current density in the cross section of the wire. The vortex tubes corresponding to the current-induced H_φ field are rings coaxial with the wire. Above a critical current, these vortex rings enter at the edge of the cylinder and shrink until they annihilate on the axis of the cylinder. This process repeats and leads to dissipation. There is no stable mixed state associated with a H_φ field unless the vortex rings are pinned by impurities in the material. Blackburn *et al.* [7] have argued that by entangling the vortex rings with vortex lines due to a strong longitudinal field, the rings can be prevented from shrinking and thereby increase the critical current in the wire.

We model a cylindrical shape of the wire in a rectangular box by adding a potential term $V\psi$ with $V = 5$ to Eq. (9) at all grid points outside a cylindrical region with radius

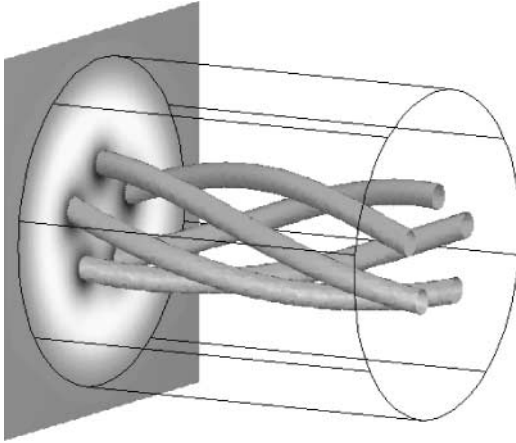


FIG. 3. Time-independent arrangement of spiral vortices in a cylinder of radius 12ξ , $\kappa = 5$, $\sigma = 1$. Five vortex lines are entangled with two rings. The applied fields are $H_z = 0.2$ and $H_\phi = 1.5/\rho$, respectively. The tubes show the density of the order at the level $|\psi|^2 = 0.3$. The left slice shows the magnetic field component parallel to the wire, H_z . Dark regions indicate a high field. The black lines mark the boundaries of the wire.

$R = 12\xi$. The density of the order parameter outside the cylinder decreases rapidly to zero. An array of longitudinal vortex tubes is created by imposing boundary conditions for an external magnetic parallel to the wire. A current is ramped up by slowly increasing a circular field (B_x and B_y) around the box until vortices enter. The Bean–Livingston surface barrier was lowered by adding a weak sinusoidal potential at the surface of the cylinder. Figure 3 shows a time-independent state that arises after two vortex rings have entered the cylinder and entangled with the vortex lines. The critical current is dominated by the surface barrier, as expected for small samples. Consequently, we do not observe any improvement in the critical current due to the presence of a longitudinal field. However, the effect could become more significant for larger sample sizes or if the surface effects are suppressed [16].

4. EXAMPLE 2: WIRE WITH TRANSVERSE FIELD

In superconducting magnets, the external magnetic field is typically aligned perpendicular to the wire (B_x , for example). In the mixed state, an array of vortex lines fills up the superconductor (see Fig. 4). Any current carried by the wire superimposes a circular field onto this applied field. As a result, a gradient of the magnetic field develops that can be associated with a Lorentz force on the vortices. In most applications, different pinning mechanisms balance this Lorentz force and freeze the flux lattice up to a critical current density. For larger currents, the Lorentz force exceeds the pinning force and vortices start moving [16]. The motion of the flux lattice coincides with the breakdown of superconductivity.

In this geometry the magnetic field at the boundary of the computational box strongly depends on the currents inside unless the box size is much larger than the radius R of the cylinder. In the Meissner state, for example, no flux lines penetrate the wire and supercurrents in the surface of the superconductor cancel the external field in the bulk of the wire. The field lines of these surface currents also extend outside the sample at length scales of order R . In the mixed state, the induced field is smaller and can be regarded as a small correction. To find a self-consistent solution, the fields induced by both the supercurrents and normal

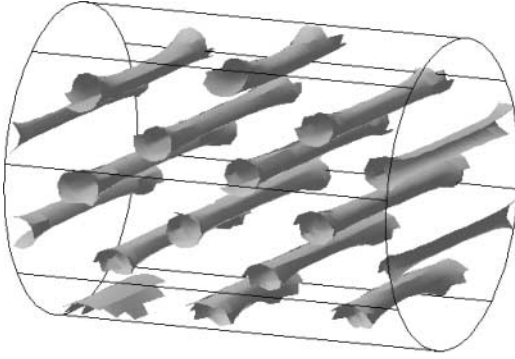


FIG. 4. Array of vortices in a wire exposed to a perpendicular magnetic field $B_x = 0.4$. The vortices tubes enter and exit the surface of the superconductor normally. The Ginzburg–Landau parameter is $\kappa = 5$; the radius of the wire $R = 8\xi$; and $\sigma = 1$.

currents have to be added to the applied field and included in the boundary conditions at each time step. We calculate the induced field $\mathbf{H}_{\text{ind}}(\mathbf{r})$ using the Biot–Savart law, which in our units has the form

$$\mathbf{H}_{\text{ind}}(\mathbf{r}) = \frac{1}{4\pi\kappa^2} \int d^3r' \mathbf{j}(\mathbf{r}') \times \frac{\mathbf{r} - \mathbf{r}'}{|\mathbf{r} - \mathbf{r}'|^3}. \quad (38)$$

This calculation is computationally expensive. The integral is approximated by summing over all grid points for each boundary point requiring a total of $\mathcal{O}(N^5)$ calculations, whereas a time step takes $\mathcal{O}(N^3)$ calculations for a box of N^3 grid points. With periodic boundary conditions, the integration must also be extended to regions outside the box. The effect of including \mathbf{H}_{ind} is to bend the vortex lines, especially near the top and the bottom of the sample, as is apparent in Fig. 4. To model the motion of flux lines, a fully self-consistent time-dependent solution can be found by iterating the boundary conditions at each time step. However, in practice the study of the motion of vortices above the critical current does not seem to be feasible. Possible ways around this problem are to increase the box size so that the induced currents can be neglected, to cutoff the integral in (38) at a certain distance from the boundary, $|\mathbf{r} - \mathbf{r}'| < \mathcal{R}$, or to update $\mathbf{H}_{\text{ind}}(\mathbf{r})$ only in larger intervals rather than at every time step. The latter approach is especially suitable for finding time-independent solutions.

5. CONCLUDING REMARKS

In summary, we have demonstrated the use of a semi-implicit finite-difference scheme to solve the three-dimensional time-dependent Ginzburg–Landau equations. The method converges if a Crank–Nicholson scheme is applied to all Laplacian-type terms while all other terms are treated explicitly. We iterate each time step to achieve second-order accuracy in time. For intermediate values of the Ginzburg–Landau parameter κ , the method is stable and accurate for time steps two orders of magnitude larger than those used in the standard explicit schemes. If the magnetic field at the surface of the computational box is partly due to currents inside, a self-consistent solution can be found by iteration. However, a full Biot–Savart calculation of the induced magnetic field remains computationally expensive.

ACKNOWLEDGMENT

We thank EPSRC for financial support of this project.

REFERENCES

1. W. D. Groppe, *et al.*, Numerical simulation of vortex dynamics in type-II superconductors, *J. Comput. Phys.* **123**, 254 (1996).
2. H. Frahm, S. Ulah, and A. T. Dorsey, Flux dynamics and the growth of the superconducting phase, *Phys. Rev. Lett.* **66**, 3067 (1991).
3. R. Kato, Y. Enomoto, and S. Maekawa, Computer simulations of dynamics of flux lines in type-II superconductors, *Phys. Rev. B* **44**, 6916 (1991).
4. M. Machida and H. Kaburaki, Direct simulation of the time-dependent Ginzburg–Landau equation for type-II superconducting thin films: Dynamics and V-I characteristics, *Phys. Rev. Lett.* **71**, 3206 (1993).
5. G. W. Crabtree, *et al.*, Numerical simulations of driven vortex systems, *Phys. Rev. B* **61**, 1446 (2000).
6. E. Coskun and M. K. Kwong, Simulating vortex motion in superconducting films with the time-dependent Ginzburg–Landau equations, *Nonlinearity* **10**, 579 (1997).
7. J. F. Blackburn, A. Campbell, and E. K. H. Salje, The force-free case in three-dimensional superconductors: a computational study, *Philos. Mag. B* **80**, 1455 (2000).
8. Q. Du, Finite element method for the time dependent GL model of superconductivity, *Comp. Math. Appl.* **27**, 119 (1994).
9. Q. Du, M. D. Gunzburger, and J. S. Peterson, Solving the Ginzburg–Landau equations by finite-element methods, *Phys. Rev. B* **46**, 9027 (1992).
10. L. Q. Chen and J. Shen, Applications of semi-implicit Fourier-spectral method to phase field equations, *Comp. Phys. Commun.* **108**, 147 (1998).
11. T. Winiecki and C. S. Adams, Motion of an object through a quantum fluid, *Europhys. Lett.* **52**, 257 (2000); M. Leadbeater, T. Winiecki, D. C. Samuels, C. F. Barenghi, and C. S. Adams, Sound emission due to superfluid vortex reconnections, *Phys. Rev. Lett.* **86**, 1410 (2001).
12. W. F. Ames, *Numerical Methods for Partial Differential Equations* (Academic Press, San Diego, 1992).
13. W. H. Press, S. A. Teukolsky, W. T. Vetterling, and B. P. Flannery, *Numerical Recipes in Fortran—The Art of Scientific Computing* (Cambridge Univ. Press, Cambridge, UK, 1992), 2nd ed.
14. Y. A. Genenko, Magnetic self-field entry into a current-carrying type-II superconductor. II. Helical vortices in a longitudinal magnetic field, *Phys. Rev. B* **51**, 3686 (1995).
15. B. C. Belonger and M. A. R. LeBlanc, Interaction of conduction and induced currents in Nb₃Zr wires subjected to axial fields, *Appl. Phys. Lett.* **10**, 298 (1967).
16. T. Winiecki and C. S. Adams, Time-dependent Ginzburg–Landau simulations of the voltage–current characteristic of type-II superconductors with pinning, *Phys. Rev. B* **65**, 104517 (2002).